

# Optimal harvesting of lipids-rich microalgae subject to a circadian cycle under limited nitrogen supply

V. Marquez<sup>1</sup>, A.J. Beccaria<sup>1</sup> and R.G. Dondo<sup>1,2,\*</sup>

<sup>1</sup>Laboratorio de Fermentaciones. Facultad de Bioquímica y Ciencias Biológicas, Universidad Nacional del Litoral, Paraje El Pozo s/n, (3000), Santa Fe, Argentina

<sup>2</sup>Instituto de Desarrollo Tecnológico para la Industria Química (INTEC), Güemes 3450, (3000) Santa Fe, Argentina

\*Corresponding author: rdondo@santafe-conicet.gov.ar

**ABSTRACT** The harvesting of algae rich in triacylglycerol from an open raceway pond with volume-changes synchronized to the circadian cycle and under limited nitrogen supply is researched. A reduced metabolic model of its non-balanced growth is embedded into a macroscopic balance for simulating growth in such a type of bioreactor. Afterwards, the model is used jointly with optimal control to derive cyclic inlet and outlet flow policies as well as optimal nitrogen levels for different time-horizons and initial physiological states in a case study which uses bibliographic data for the *Tisochrysis lutea* alga.

**KEYWORDS** Single cell oil; Metabolic network; Non-balanced growth; Optimal control

## 1. Introduction

Bioprocessing is used extensively for the production, from living cells, of high value bioproducts like nutrition supplements, pharmaceuticals and biofuels (Nolasco et al., 2021). Single-cell photoautotrophic microorganisms which convert photons into cellular energy and capture carbon dioxide have been subject of growing research. Eukaryotic (microalgae) or prokaryotic (cyanobacteria) microorganisms can synthesize products of industrial interest such as, proteins, polysaccharides, lipids, vitamins and pigments. These microorganisms mainly require water, light, and inorganic nutrients to grow and they do not compete with food production for resources such as land and water. Mathematical modeling coupled with optimal control can help to optimize these complex biological systems because it allows exploiting its biological mechanisms to increase productivity. Open raceway pond (ORP), which is one of the oldest and simplest photobioreactor types, is known to be one of the most suitable systems for large-scale microalgae production given its minimal capital and operating costs, low electric energy requirement for their functioning and easy to scale up (Narala et al., 2016). As autotrophic algae subject to circadian cycles store energy and carbon during the day to support growth and maintenance during the night, optimizing cyclic harvesting policies should be a research priority, but to the best of our knowledge, the paper by Bayen et al. (2015) is the only one that researched this subject. The authors researched an optimal control problem for optimizing the production of methane in a digester with the dilution rate as control variable by using a relatively simple unstructured model of the system. Baroukh et al. (2014) derived a core carbon metabolic network common

to unicellular photoautotrophic microalgae containing the central metabolic pathways (photosynthesis, glycolysis, pentose-phosphate pathway, citric acid cycle, oxidative phosphorylation, chlorophyll, carbohydrates, amino acid and nucleotide synthesis). The authors did not represent species-specific pathways such as the synthesis of secondary metabolites since they assumed these pathways to have negligible fluxes compared to main pathways. This model may be helpful for optimizing the production of lipids by microalgae subject to photoperiodic illumination. Nevertheless, applying optimal control to this biotechnological system is not easy because of the need of adequately represent the day-night cycle and optimizing several controllable variables which have different time-scale impacts into the microbial metabolism.

This paper is concerned with the optimal control of a variable-volume ORP producing lipids useful as raw material for biodiesel. Numerical research on a case study with bibliographic information is presented.

## 2. Modeling metabolism subject to circadian cycles

Unstructured biotechnological models have limited biological insights while the utilization of structured models opens the door to a quantitative analysis of the intracellular metabolic mechanisms. Flux Balance Analysis is a constraint-based modeling approach representing the steady state mass and energy balances within the cell. It assumes that the extracellular environment of the cell culture is constant. This is not the case for circadian processes and this hypothesis, usual in metabolic engineering, is unsuitable for microorganisms subject to photoperiodic cycles because they store energy and carbon during the day to support growth and maintenance during the night. As the autotrophic metabolism results synchronized with the circadian cycle, intermediate metabolites such as carbohydrates and lipids accumulate during the day and are consumed during the night (Lacour et al., 2012). To model this behavior some metabolites can be

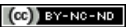
Copyright © 2024 Latin American Applied Research

DOI: 10.52292/j.laar.2024.1144

Received: August 8, 2022.

Accepted: May 16, 2023.

Recommended by Mariano Martin Martin.

 This work is licensed under a Creative Commons Attribution-NonCommercial-NoDerivatives 4.0 International License.

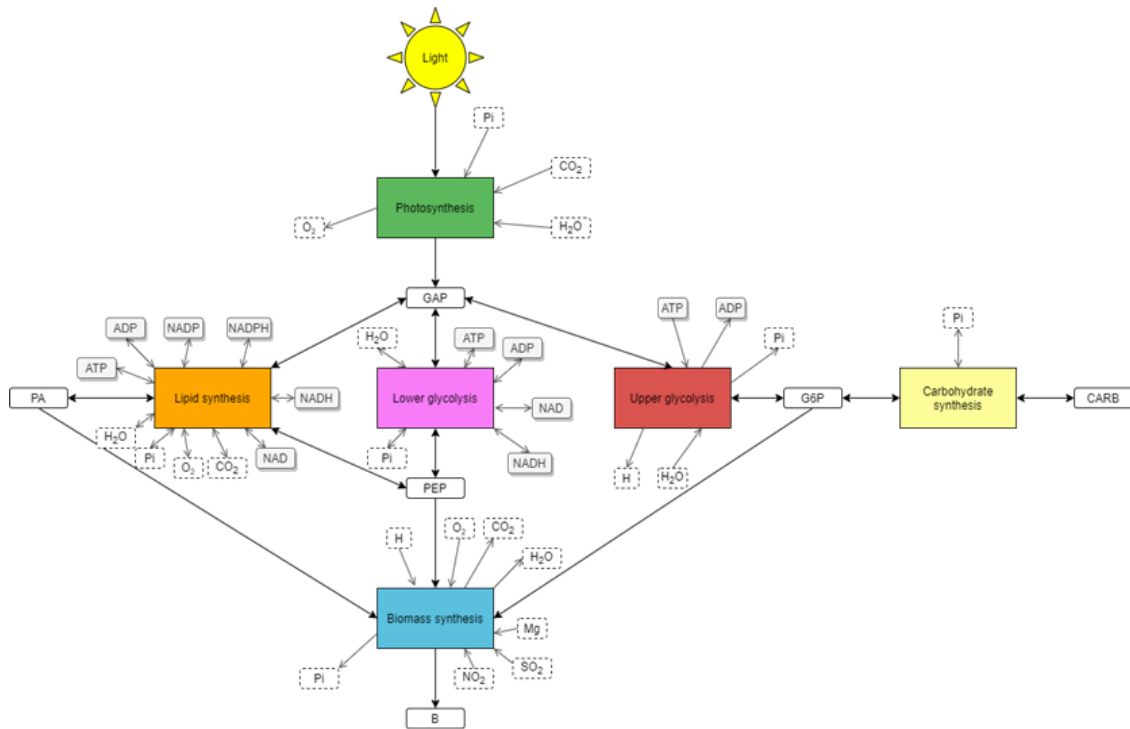


Figure 1: Metabolic network for generic unicellular photoautotrophic microalgae.

seen as products during the day and substrates during the night. In this way, metabolic modeling may still be possible in order to understand the microalgae metabolism submitted to day/night cycles. Dynamic Reduction of Unbalanced Metabolism (Baroukh et al., 2014) is a proposal that intends to conciliate macroscopic and metabolic modeling scales by deriving from a metabolic network the dynamics of macroscopic variables and the accumulation of intracellular metabolites. This framework allows modeling intracellular processes under non-balanced growth submitted to circadian cycles for non-limiting nitrogen conditions and under nitrogen starvation conditions. The model was expressed as eight macroscopic reactions representing an intracellular network and is depicted by Fig. 1.

A reduced model described by eight macroscopic reactions and 21 metabolites was presented where functional biomass and photons are represented as metabolites. The description of the metabolic network is summarized by the Table 1. For each macroscopic reaction, simple first order kinetics were proposed. In this way, six sub-networks were obtained: i) photosynthesis, ii) upper glycolysis, iii) carbohydrate synthesis, iv) lower glycolysis, v) lipids synthesis, vi) biomass synthesis.

Note that upper glycolysis comprises three macroscopic reactions. The information about the reactions network is compacted into the stoichiometric matrix  $K'$ , where rows correspond to key metabolites and columns correspond to macroscopic reactions.  $K'$  may be divided into sub-matrixes  $K'_S$ ,  $K'_A$  and  $K'_B$  shown in Table 2 which corresponds to substrates  $S = \text{Ligth}, \text{CO}_2, \text{O}_2, \text{Pi}$ -orthophosphate-,  $\text{SO}_4, \text{NO}_3, \text{Mg}, \text{H}_2\text{O}, \text{H}$ , intracellular metabolites  $A = \text{ATP}$  –adenosine triphosphate–,  $\text{ADP}$  –adenosine diphosphate–,  $\text{NADH}$  –nicotinamide reduced–,

$\text{NAD}$  –nicotinamidephosphate oxidized–,  $\text{NADP}$  –Nicotinamidephosphate oxidized–,  $\text{NADPH}$  –nicotinamidephosphate reduced–,  $\text{GAP}$  –glyceraldehyde-3-phosphate–,  $\text{G6P}$  –glucose-6-phosphate–,  $\text{PEP}$  –glucose-6-phosphate–,  $\text{CARB}$  –carbohydrates–,  $\text{TAG}$  –triacylglycerol–, and functional biomass  $B$  respectively.

We assume that energy cofactors  $\text{ATP}, \text{ADP}, \text{NADH}, \text{NAD}, \text{NADP}, \text{NADPH}$  are in pseudo steady-state and their mass contribution to total biomass are assumed as negligible compared to storable intracellular molecules ( $\text{CARB}, \text{TAG}, \text{PEP}, \text{G6P}, \text{GAP}$ ).

The availability of nitrogen into the cells plays a crucial role on the synthesis of intracellular metabolites and on the release of extracellular organic mass and it is expected to impact extensively on the harvesting operation (Baroni et al., 2020). There are two main hypotheses to explain the deviation of intracellular carbohydrates and lipids levels in conditions of nitrogen starvation with respect to non-limiting nitrogen conditions: i) Excretion of some carbon compounds during nitrogen starvation with a constant inorganic carbon flux. ii) Dissipation of light to down regulate the flux of inorganic carbon. Hence, during nitrogen starvation, microalgae might use these mechanisms to protect themselves from the light surplus and from the excess of carbon coming into their metabolism. The excretion hypothesis relies on the fact that excretion of intracellular compounds was observed for some microalgae during nutrient depleting conditions (Underwood et al., 2004). The phenomenon of excretion is microalgae-dependent. The dissipation hypothesis relies on the fact that microalgae have dissipation mechanisms at the level of photosynthesis to vent the energy surplus (Klok et al., 2013; Nogales et al., 2012). The kinetics for

Table 1: Sub-networks for metabolic reactions of generic unicellular autotrophic microalgae.

| Sub-network            | Macroscopic reaction               | Stoichiometry  | Kinetics                        |
|------------------------|------------------------------------|--|---------------------------------|
| Photosynthesis         | MR <sub>1</sub>                    | 30 Light + 3 CO <sub>2</sub> + 2 H <sub>2</sub> O + Pi → GAP + 3 O <sub>2</sub>  | rMR1 = kMR1*I                   |
| Upper glycolysis       | MR <sub>2</sub><br>Futile cycle    | ATP + H <sub>2</sub> O ↔ ADP + Pi + H  | rMR2 = 0                        |
|                        | MR <sub>3</sub><br>G6P synthesis   | 2 GAP + H <sub>2</sub> O → G6P + Pi  | rMR3 = kMR3*GAP                 |
|                        | MR <sub>4</sub><br>G6P consumption | G6P + ATP → H + ADP + 2 GAP  | rMR4 = kMR4*G6P                 |
| Lower glycolysis       | MR <sub>5</sub>                    | GAP + ADP + Pi + NAD ↔ PEP + ATP + NADH + H <sub>2</sub> O + H   | rMR5 = kMR5*GAP - k'MR5*PEP     |
| Carbohydrate synthesis | MR <sub>6</sub>                    | G6P ↔ CARB + Pi  | rMR6 = kMR6*G6P - k'MR6*CARB    |
| Lipids synthesis       | MR <sub>7</sub>                    | GAP + 16.61 PEP + 2 ADP + 13.46 NAD + 29.3 NADPH + 34.48 H + 2.15 O <sub>2</sub> ↔ TAG + 14.61 Pi + 2 ATP + 13.46 NADH + 29.3 NADP + 4.31 H <sub>2</sub> O + 16.61 CO <sub>2</sub> | rMR7 = kMR7*PEP*GAP - k'MR7*TAG |
| Biomass synthesis      | MR <sub>8</sub>                    | 3.13 PEP + 7.37 O <sub>2</sub> + 4.46 H + 1.31 NO <sub>3</sub> + 1.14 G6P + 0.11 TAG + 0.03 SO <sub>4</sub> + 0.0025 Mg → B + 11.67 CO <sub>2</sub> + 4.23 Pi + 6 H <sub>2</sub> O | rMR8 = kMR8*PEP*G6P*NO3         |

Table 2: Stoichiometric matrix  $K'$  and submatrixes  $K'_S$ ,  $K'_A$  and  $K'_B$ .

|     |                  | MR <sub>1</sub> | MR <sub>2</sub> | MR <sub>3</sub> | MR <sub>4</sub> | MR <sub>5</sub> | MR <sub>6</sub> | MR <sub>7</sub> | MR <sub>8</sub> |
|-----|------------------|-----------------|-----------------|-----------------|-----------------|-----------------|-----------------|-----------------|-----------------|
| KS' | Ligth            | -30             |                 |                 |                 |                 |                 |                 |                 |
|     | CO <sub>2</sub>  | -3              |                 |                 |                 |                 |                 | 16.61           | 11.67           |
|     | O <sub>2</sub>   | 3               |                 |                 |                 |                 | 1               | -2.15           | -7.37           |
|     | Pi               | -1              | 1               | 1               |                 | -1              |                 | 14.51           | 4.23            |
|     | SO <sub>4</sub>  |                 |                 |                 |                 |                 |                 |                 | -0.03           |
|     | NO <sub>3</sub>  |                 |                 |                 |                 |                 |                 |                 | -1.31           |
|     | Mg               |                 |                 |                 |                 |                 |                 |                 | -0.025          |
|     | H <sub>2</sub> O | -2              | -1              | -1              |                 | 1               |                 | 4.31            | 6               |
| KA' | H                |                 | 1               |                 | 1               | 1               |                 | -34.38          | -4.46           |
|     | ATP              |                 | -1              |                 | -1              | 1               |                 | 2               |                 |
|     | ADP              |                 | 1               |                 | 1               | -1              |                 | -2              |                 |
|     | NADH             |                 |                 |                 |                 | 1               |                 | 13.46           |                 |
|     | NAD              |                 |                 |                 |                 |                 |                 | -13.46          |                 |
|     | NADP             |                 |                 |                 |                 | -1              |                 | -29.3           |                 |
|     | NADPH            |                 |                 |                 |                 |                 |                 | 29.3            |                 |
|     | GAP              | 1               |                 | -2              | 2               | -1              |                 | -1              |                 |
|     | G6P              |                 |                 | 1               | 1               |                 | 1               |                 | -1.14           |
|     | PEP              |                 |                 |                 |                 | 1               |                 | -16.61          | -3.13           |
| KB' | CARB             |                 |                 |                 |                 |                 | 1               |                 |                 |
|     | TAG              |                 |                 |                 |                 |                 |                 | 1               | -0.11           |
| KB' | B                |                 |                 |                 |                 |                 |                 |                 | 1               |

both mechanisms are modeled as follows:

$$r_{excr} = k_{excr} \max\left(\frac{X_C/B}{Q_{excr}^{min}}; 0\right) PEP \quad (1)$$

$$r_{MR1} = k'_{MR1} \left(1 - \frac{X_C/B}{Q_r^{max}}\right) I \quad (2)$$

where both the excretion or the dissipation kinetics depends on the  $X_C/B$  ratio of the cell, being  $X_C$  the fraction of carbon in total biomass and  $B$  the concentration of

functional-biomass. According to Eq. 1, excretion of PEP would only starts when  $X_C/B$  reaches a minimum threshold ( $Q_{excr}^{min}$ ) and increases proportionally with  $X_C/B$  once this threshold has been reached. Excretion of any other component would have the same type of kinetics. In the same way, the kinetic function 2 would be modulated by the  $X_C/B$  ratio and the rate  $MR_1$  will be approaching to zero when this ratio approaches to the threshold  $Q_r^{max}$ . In summary, the autotrophic metabolism of algae is modeled by the reaction network shown in Tables 1 and 2 plus the excretion kinetics given by Eq. 1 or the dissipation kinetics defined by Eq. 2.

### 3. Cyclic volume-varying continuous operation mode

For production of lipids for biofuels from microalgae, the composition of the harvested culture must be optimized to obtain the maximum feasible quantity of TAGs. In order to build a model for optimizing the harvesting of lipids from algae subject to a circadian cycle and under nitrogen starvation, the metabolic model above presented must be embedded into macroscopic balances corresponding to the operation mode of the ORP. Furthermore, the objective, the states and the control variables must be defined. The continuous operation mode usually has been regarded as the most efficient, but it is not well suited to synchronize with autotrophic reactions aligned to the circadian cycle. On the other hand, a cyclic fed-batch operation can synchronize culture conditions and volume variations with day-night cycles. Because of feeding of a nutrient solution, the culture volume increases and if it is possible to control the outlet flow and retain a portion of a fed-batch culture of the end of one cycle to use the residual part as inoculum for the next cycle, this operation mode is called repeated fed-batch or variable-volume continuous-reactor –VCCR– (Asenjo and Merchuk, 1995). This mode can be synchronized to the circadian cycle by varying the culture volume via the control of inlet and outlet flows. Also, nitrogen starvation allows to flow the photosynthesis' energy into molecules which do not contain nitrogen. Nitrogen levels can be controlled by manipulating the concentration of the nitrogen source in the inlet flow. In summary, the macroscopic model corresponding to a VCCR operation mode with controlled nitrates concentration can be described by the following system of ordinary differential equations (ODEs):

$$\frac{d}{dt} \begin{pmatrix} NO_3 \\ CARB \\ TAG \\ PEP \\ G6P \\ GAP \\ B \end{pmatrix} = \begin{pmatrix} r_{NO_3} \\ r_{CARB} \\ r_{TAG} \\ r_{PEP} \\ r_{G6P} \\ r_{GAP} \\ r_B \end{pmatrix} B - \frac{F_i}{V} \begin{pmatrix} NO_3 \\ CARB \\ TAG \\ PEP \\ G6P \\ GAP \\ B \end{pmatrix} + \frac{F_i}{V} \begin{pmatrix} NO_3^{in} \\ 0 \\ 0 \\ 0 \\ 0 \\ 0 \\ 0 \end{pmatrix} \quad (3)$$

The dynamics of the culture volume is given by:

$$\frac{dV}{dt} = F_i - F_o \quad (4)$$

As it is assumed that excretion doesn't have any effect into the intracellular kinetics, the balance of excreted PEP would be given by Eq. 5:

$$\frac{dPEP_{excr}}{dt} = r_{excr}B - \frac{F_i}{V}PEP_{excr} \quad (5)$$

Any other excreted component different from PEP would have the same kind of balance equation. Here, CARB, TAG, PEP, G6P and GAP are macroscopic concentrations of intracellular compounds;  $B$  is the macroscopic concentration of functional biomass,  $NO_3/NO_3^{in}$  are the concentration of nitrates in the culture/feed-flow respectively and  $F_i/F_o$  are the culture inflow/outflow. For the remaining metabolites, the quasi-steady-state assumption is taken as activities of these compounds are not explicitly considered in kinetics of Table 1. The rates-vector  $r = [r_{NO_3}, r_{CARB}, r_{TAG}, r_{PEP}, r_{G6P}, r_{GAP}, r_B]$  represents the net production of the respective components and is computed as follows:

$$r = K_{stoich}\Lambda \quad (6)$$

where  $K_{stoich}$  is the matrix of stoichiometric coefficients built by taking rows associated to component  $NO_3(t)$ ,  $CARB(t)$ ,  $TAG(t)$ ,  $PEP(t)$ ,  $G6P(t)$ ,  $GAP(t)$ ,  $B(t)$ , from matrix  $K'$ . The vector of independent intracellular reactions is denoted by  $\Lambda = [r_{MR_1}, \dots, r_{MR_8}]$ . The photons inflow is computed by interpolation between points provided by a table expressed as follows:

$$I_t = I(t) \quad (7)$$

that summarizes illumination data plots as the one depicted in Figure 2, which represents 5 ideal unclouded summer days, where  $t$  is the time and  $t = 0$  h correspond to the sunrise.

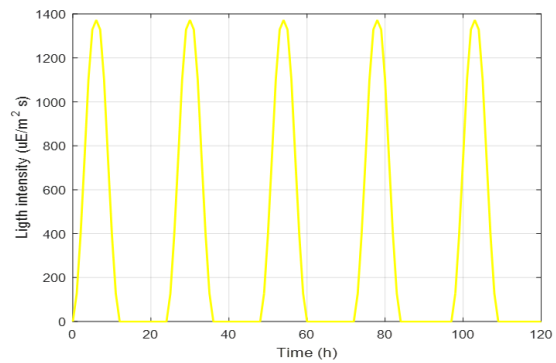


Figure 2: Typical daily light intensity.

The total biomass, which has a variable composition, is computed by:

$$X(t) = \sum_e \sum_A (e_A A(t) + e_B B(t)) \quad (8)$$

$$A \in \{CARB; TAG; PEP; G6P; GAP\}$$

$$e \in \{C; H; O; N; P; S\}$$

where  $e_A$  and  $e_B$  correspond to the number of atoms of element  $e$  per mol of  $A$  and mol of  $B$ , respectively while

Table 3: Elemental composition of intracellular compounds and functional biomass.

|      | C    | H     | O    | N    | P    | S     |
|------|------|-------|------|------|------|-------|
| GAP  | 3    | 7     | 6    | 0    | 1    | 0     |
| G6P  | 6    | 13    | 9    | 0    | 1    | 0     |
| PEP  | 3    | 5     | 6    | 0    | 1    | 0     |
| CARB | 6    | 10    | 5    | 0    | 0    | 0     |
| TAG  | 36.2 | 63.4  | 8    | 0    | 1    | 0     |
| B    | 8.59 | 14.13 | 2.49 | 1.26 | 0.15 | 0.025 |

$A(t)$  and  $B(t)$  correspond to the concentration of  $A$  and functional biomass  $B$  at time  $t$ . Elemental composition of compounds grouped on  $A$  are specified on rows of the matrix presented in Table 3.

Microalgae cultures are usually carried out in two steps. First, microalgae are grown in optimal growth conditions until a high biomass concentration is reached. Then, TAGs accumulation is triggered by nitrogen starvation. However, to further improve productivity, the culture conditions should be optimally controlled. This opens the door for using optimal control in order to compute the best way for manipulating environmental conditions. Optimal control is a branch of optimization that deals with finding controls of a dynamical system over a fixed or free time-period. It includes a cost functional that is a function on state and control variables, a set of differential equations describing the system dynamics and algebraic equations stating hardware characteristics and constraints to the dynamic system. It can be defined as follows:

Maximize

$$J = G(x(t_f), x(t_0)) + \int_0^{t_f} F(x(t), u(t)) dt \quad (9)$$

subject to:

$$\frac{dx}{dt} = f(x(t), u(t)) \quad x(0) = x_0 \quad (10)$$

$$S^{Min}(t) \leq S(x(t)) \leq S^{Max}(t) \quad (11)$$

$$C^{Min}(t) \leq C(u(t)) \leq C^{Max}(t) \quad (12)$$

where Eq. 10 states the dynamic of the process, Eq. 11 set states and path constraints, Eq. 12 set control variable constraints; and  $x(t)$ ,  $u(t)$  and  $t$  are respectively the state-variables vector, the control-variables vector and the time. As biodiesel is produced from lipids, the objective function 9 is rewritten as the maximization of the quantity of harvested TAGs along the whole culture time:

Maximize

$$\int_{t=0}^{t_f} (F_o(t) TAG(t)) dt \quad (13)$$

The dynamics of intracellular components and functional biomass under no nitrogen-starvation conditions are defined by Eqs. 3. The dynamics of the culture volume is represented by Eq. 4. Equation 5 defines the dynamics of excretion. Furthermore, with this hypothesis,  $r_{PEP}$  must be replaced by  $(r_{PEP} - r_{excr})$  in Eq 3 in order to

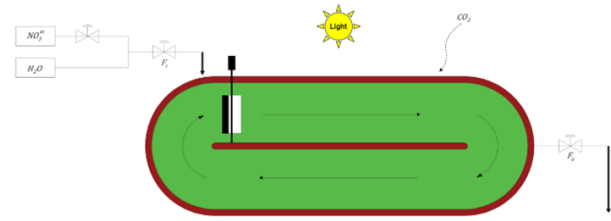


Figure 3: Representation of a VVCR type ORP for culturing of microalgae.

consider the effect of intracellular dilution caused by the excretion process. For the model corresponding to the dissipation hypothesis, Eq. 5 is deleted and Eq. 2 replaces the kinetic equation corresponding to the reaction  $MR_1$  shown in Table 1. So, the states-vector is given by  $x(t) = \{NO_3(t), CARB(t), TAG(t), PEP(t), G6P(t), GAP(t), B(t), V(t), PEP_{excr}(t)\}$  if we consider the excretion hypothesis or by  $x(t) = \{NO_3(t), CARB(t), TAG(t), PEP(t), G6P(t), GAP(t), B(t), V(t)\}$  if we consider the dissipation hypothesis. The following assumptions allowed considering the above-described dynamic models: (i) The VVCR culture is homogeneous and perfectly mixed. (ii) Evaporation effects are negligible. In a VVCR, both the inlet  $F_i(t)$  and the outlet  $F_o(t)$  flows can be manipulated. In addition, to induce nitrogen starvation, the concentration of nitrate,  $NO_3^{in}(t)$ , in the inlet flow must be controlled. So, the vector of control variables would be given by  $u(t) = F_i(t), F_o(t), NO_3^{in}(t)$ . Fig. 3 shows a representation of an ORP used as a VVCR system with these three control variables.

Bounds for the control variables depend on the ORP hardware and are formally defined as follows:

$$\begin{aligned} 0 &\leq F_i(t) \leq F_i^{max} \\ 0 &\leq F_o(t) \leq F_o^{max} \\ 0 &\leq NO_3^i(t) \leq NO_3^{imax} \end{aligned} \quad (14)$$

The following constraint, which imposes the ORP volume as an upper bound to the culture volume must be enforced over the whole optimization time-horizon:

$$0 \leq V(t) \leq V^{max} \quad (15)$$

Realistic optimal control problems usually do not have analytic solutions and it is necessary to employ numerical methods to solve them. The GPOPS software (Rao et al., 2010), which implements the Radau pseudo-spectral collocation method, was developed in response to a growing demand from the research and academic community for an optimal control software able to solve complex optimal control problems. Its freeware 5.2-version was employed in this work.

#### 4. Numerical results for an ORP culturing *Tisochrysis lutea*

In this section, the harvesting of TAGs from a VVCR-operating ORP culturing *T. lutea* is numerically optimized. The experimental data were taken from (Lacour et al.,

Table 4: Kinetic parameters, state constraints and control constraints.

| Parameter               | Value   | Units   |
|-------------------------|---|---|
| $k_{MR1}$               | $1.1 \cdot 10^{-3}(\text{Excretion})/1.5 \cdot 10^{-3}(\text{Dissipation})$ | $\mu\text{E} (\text{m}^2 \text{ s mol h M B})^{-1}$ |
| $k_{MR3}$               | 223.53  | $(\text{h mol B})^{-1}$                             |
| $k_{MR4}$               | 10.30   | $(\text{h mol B})^{-1}$                             |
| $k_{MR5}$               | 436.95  | $(\text{h mol B})^{-1}$                             |
| $k'_{MR5}$              | 10.00   | $(\text{h mol B})^{-1}$                             |
| $k_{MR6}$               | 80.00   | $(\text{h mol B})^{-1}$                             |
| $k'_{MR6}$              | 6.50  | $(\text{h mol B})^{-1}$                             |
| $k_{MR7}$               | $1.50 \cdot 10^3$   | $(\text{M h M B})^{-1}$                             |
| $k'_{MR7}$              | 0.80  | $(\text{h mol B})^{-1}$                             |
| $k_{MR8}$               | $1.00 \cdot 10^4$   | $(\text{M}^2 \text{ h mol B})$                      |
| $k_{excr}$              | 8.00  | $(\text{h mol B})^{-1}$                             |
| $Q_{min}^{excretion}$   | 13.00   | mol/mol   |
| $Q_{max}^{dissipation}$ | 48.00   | mol/mol   |

| State              | Initial State |              | Minimum   | Maximum   |
|--------------------|---------------|--------------|-----------|-----------|
|                    | Depleted      | Undepleted   |           |           |
| NO <sub>3</sub>    | Free          | Free         | 0.0 g/L   | 2.0 g/L   |
| CARB               | 0.0 mol/L     | 0.0397 mol/L | 0.0 mol/L | 0.2 mol/L |
| TAG                | 0.0 mol/L     | 0.0047 mol/L | 0.0 mol/L | 0.2 mol/L |
| PEP                | Free          | Free         | 0.0 mol/L | 0.2 mol/L |
| G6P                | Free          | Free         | 0.0 mol/L | 0.2 mol/L |
| GAP                | Free          | Free         | 0.0 mol/L | 0.2 mol/L |
| B                  | 0.004 mol/L   | 0.005 mol/L  | 0.0 mol/L | 1 mol/L   |
| V                  | 1000 L        | 1605.1 L     | 0 L       | 2000 L    |
| PEP <sub>exr</sub> | 0 mol/L       | 0 mol/L      | 0         | $\infty$  |

| Control                       | Minimum | Maximum |
|-------------------------------|---------|---------|
| $F_i$                         | 0 L/h   | 100 L/h |
| $F_o$                         | 0 L/h   | 400 L/h |
| NO <sub>3</sub> <sup>in</sup> | 0 g/L   | 1 M/L   |

2012). In that work, continuous cultures of *T. lutea* (clone T-iso, CCAP 927/14) were done in duplicates in 5 liters cylindrical vessels at constant temperature (22 °C) and pH = 8.2, maintained by automatic injection of CO<sub>2</sub>. Nitrates, carbon, organic nitrogen levels, chlorophyll, total carbohydrates and neutral lipid concentrations were measured. The experiment was carried on by 8 days and a nitrogen starvation was performed from day 1 to day 5.5. Baroukh et al. (2014) tested in silico several variants of excretion and dissipation hypotheses and concluded that PEP excretion with membrane-lipids synthesis and dissipation of photons with membrane-lipids synthesis during nitrogen starvation were the two likeliest hypotheses. Kinetic parameters for the model above presented and parameters for both hypotheses are summarized in Table 4. Two states-conditions are enforced to highlight the cyclic nature of TAGs production in an ORP operating according to the VVCR mode under photoperiodic cycles: the initial and final volume and biomass concentrations must have the same values. So, the culture composition at the end-time may be considered as the composition of the culture for the start of another production run. The photons flow per unit if illuminated culture-surface corresponds exactly to the flow depicted in Fig. 2. We numerically optimized

the reactor operation for temporal horizons of 72, 96 and 120 h in search for cyclic harvesting policies, while considering initial, maximum and minimum state values and control bounds summarized in Table 4. The number of mesh refinement steps, while using GPOPS, was set to 5. Two initial “physiological states” were evaluated. First, to consider that production starts with biomass depleted from CARB and TAG, initial values for these compounds were assumed to be nil. In this way functional biomass is assumed to be initially empty from them. To determine the optimal profiles for biomass “undepleted” from intracellular CARB and TAG, we performed another set of optimization runs considering as initial states the ones corresponding to  $t = 48$  h (which were extracted from the optimization with biomass initially depleted). It is considered that biomass have reached a stationary physiological state correlated with the circadian cycle at this time. The initial conditions for both cases are also summarized in Table 4.

Results for both the excretion and the dissipation hypotheses are summarized in Table 5. The column “objective function” reports the quantity of harvested TAGs. The variable Q reports the total volume of harvested culture; i.e., the integral of the outlet flow while CPU indicates

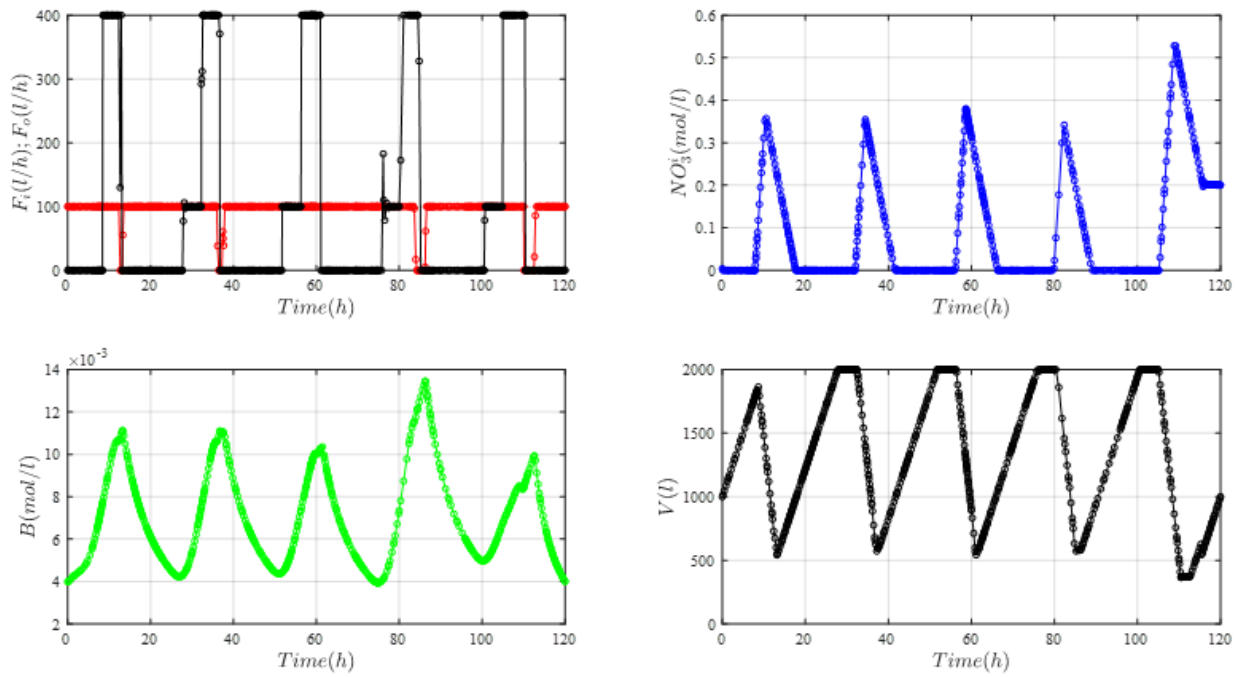


Figure 4: Optimal control profiles ( $F_i$  —;  $F_o$  —;  $NO_3^-$  —) and optimal dynamics of  $B$  (—) and  $V$  (—) for biomass initially depleted from CARB and TAG (dissipation hypothesis).

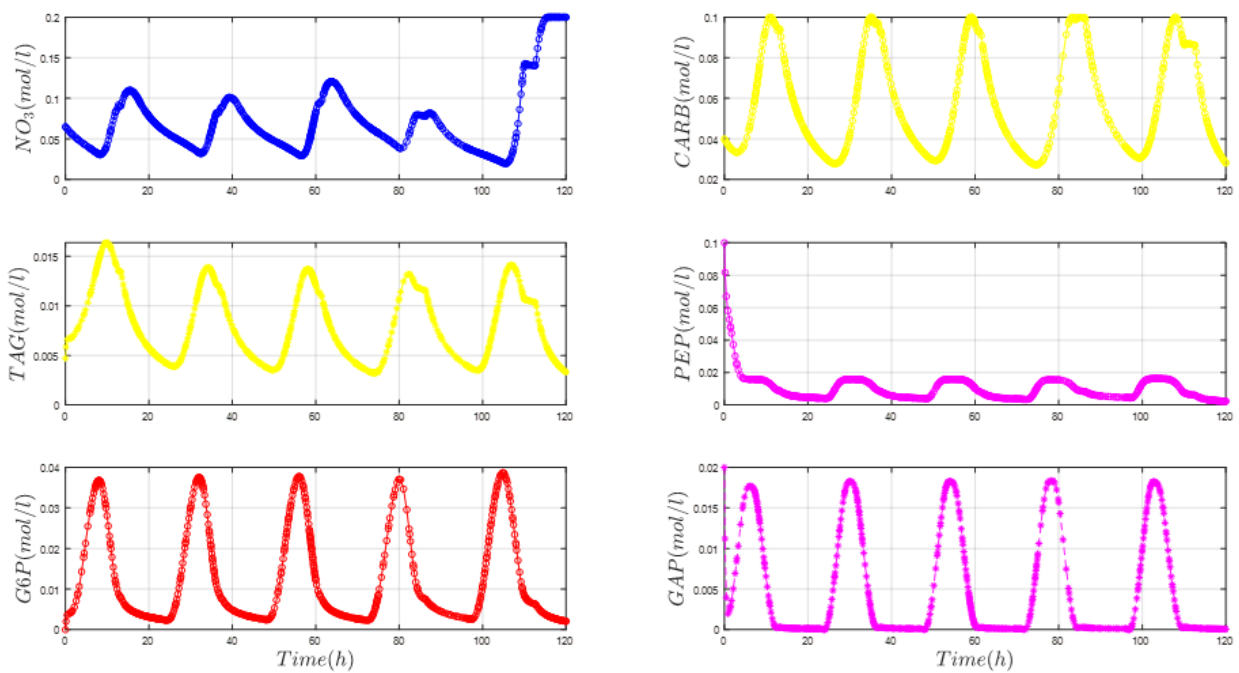


Figure 5: Optimal dynamics of intracellular states for biomass initially depleted (excretion hypothesis).

the computation time spent on an Intel® Core™ i7-CPU, 2.9 GHz, 16 GB RAM PC. Meaningful results for the dissipation hypothesis were harder to achieve because the stiffness of the ODE Eq. 2 led to a challenging optimization problem with many more collocation points than in the excretion hypothesis.

Figure 4 and 5 depict the optimal profiles of control variables for the problem solved over the 120 h time-horizon with initial conditions corresponding to the “un-

depleted” initial state and the excretion hypothesis. The optimal control policies and the dynamics of macroscopic states (concentration of functional biomass and culture volume) are illustrated in Fig. 4 while the dynamics for intracellular states are depicted in Fig. 5. Dots represent collocation points generated by GPOPS when solving the problem.

To illustrate the dynamics of the total biomass and its aggregate components, Fig. 6 depict the evolution of the

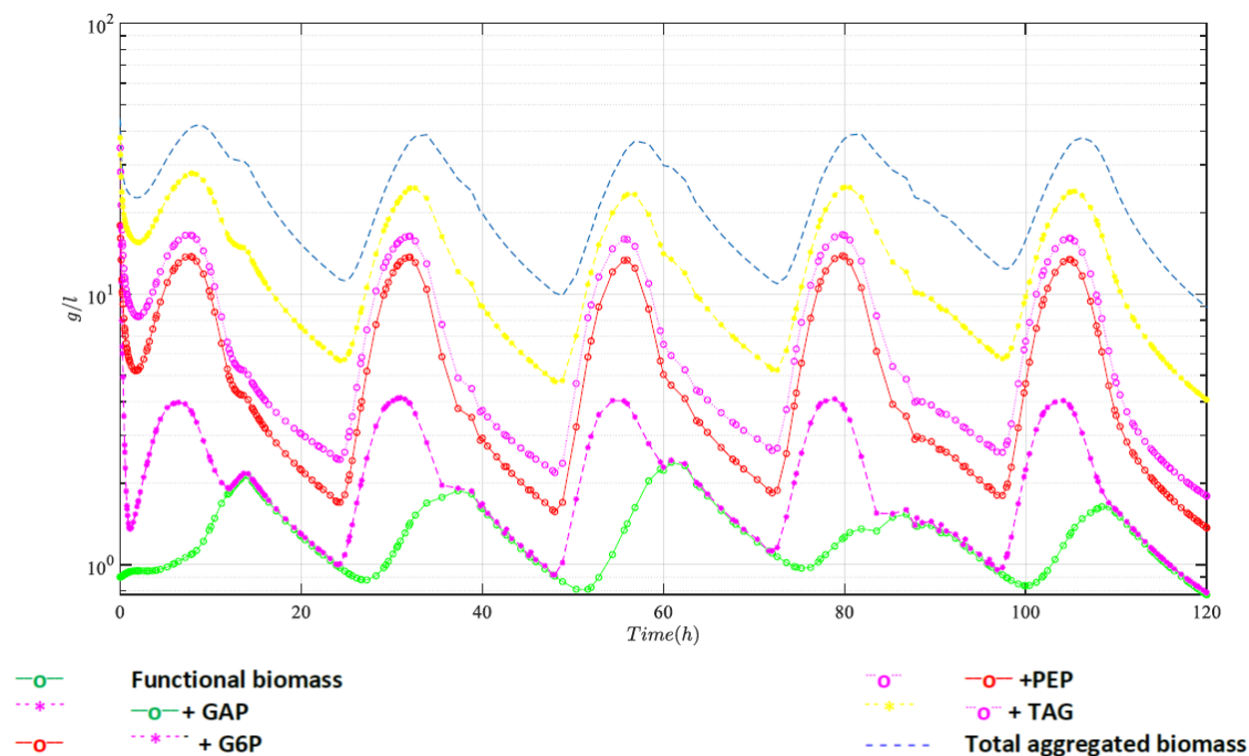


Figure 6: Dynamics of functional biomass, aggregated intracellular components and total biomass for the excretion hypothesis and “undepleted” initial states.

Table 5: Solution data for the harvesting optimization.

| Time horizon (h)                  | Objective function (mol) | Q (L) | CPU time (s) |
|-----------------------------------|--------------------------|-------|--------------|
| Excretion hypothesis              |                          |       |              |
| Initial state: Depleted biomass   |                          |       |              |
| 0-72                              | 81.89                    | 6261  | 39.4         |
| 0-96                              | 108.49                   | 8464  | 56.1         |
| 0-120                             | 134.99                   | 10592 | 172.3        |
| Initial state: Undepleted biomass |                          |       |              |
| 0-72                              | 91.53                    | 6767  | 41.1         |
| 0-96                              | 117.71                   | 8977  | 36.8         |
| 0-120                             | 144.47                   | 10971 | 59.8         |
| Dissipation hypothesis            |                          |       |              |
| Depleted biomass                  |                          |       |              |
| 0-72                              | 83.84                    | 6404  | 36           |
| 0-96                              | 111.11                   | 8688  | 50.4         |
| 0-120                             | 138.75                   | 11078 | 218.4        |
| Undepleted biomass                |                          |       |              |
| 0-72                              | 90.5                     | 6714  | 27.8         |
| 0-96                              | 117.75                   | 8975  | 37.3         |
| 0-120                             | 145.26                   | 11250 | 41.1         |

concentration of functional biomass and intracellular components. Note that the concentration of functional biomass  $B(t)$  vary between 0.7 g/L and 3 g/L while the concen-

tration of total aggregate biomass  $X(t)$  lies in the 10 g/L to 40 g/L range. So, the functional biomass constitutes roughly the 7 % of the total aggregated biomass. Control profiles derived for both hypotheses were applied to the alternative models but in all cases differences of the objective function were negligible and not distinguishable from rounding-off errors. The control profiles were remarkably similar for both hypothesis and initial conditions.

## 5. Conclusions

Metabolic modeling was seldom used jointly with optimal control because of the complexity associated to optimizing large dynamic models. Although optimizing metabolic networks in non-steady state is challenging, dynamic reduction of unbalanced metabolism allows using metabolic modeling with optimal control. In this work, a dynamic-algebraic mathematical model of production of microalgae in a VVCR-ORP, under the circadian cycle and subject to a limited nitrogen supply was developed and used to numerically optimize TAGs harvesting. The metabolic model was embedded into macroscopic balances corresponding to a VVCR operation mode and three variables were considered as control variables: the inlet flow, the outlet flow and the nitrates concentration in the inlet. Afterwards, an optimal control problem was proposed to derive optimal manipulation policies for these control variables. Optimization profiles over time-horizons of 3, 4 and 5 days for kinetic information corresponding to the *T. lutea* alga were obtained for two initial physiological states. Two mechanisms to deal with nitrogen starvation were considered and control policies were optimized to compute cyclic



harvesting policies which resulted quite similar for both initial physiological states and both hypotheses. It seems that there exists an optimal min-volume/max-volume ratio that tends to be around 1/4 for any cycle of the working timeframe. This work shows that it is possible to jointly use optimal control and dynamic metabolic modeling. As a next research step, we are currently culturing *C. Vulgaris* to obtain experimental kinetic and yield data that will allow us to derive and experimentally validate optimal harvesting policies for such a microalga.

## References

- Asenjo, J. and Merchuk, J. (1995). *Bioreactor System Design*. CRC Press.
- Baroukh, C., Muñoz-Tamayo, R., Steyer, J.-P., and Bernard, O. (2014). DRUM: A new framework for metabolic modeling under non-balanced growth. application to the carbon metabolism of unicellular microalgae. *PLoS One*, 9(8):e104499.
- Bayen, T., Mairet, F., Martinon, P., and Sebbah, M. (2015). Analysis of a periodic optimal control problem connected to microalgae anaerobic digestion. *Optim. Control Appl. Methods*, 36(6):750–773.
- Klok, A. J., Verbaanderd, J. A., Lamers, P. P., Martens, D. E., Rinzema, A., and Wijffels, R. H. (2013). A model for customising biomass composition in continuous microalgae production. *Bioresour. Technol.*, 146:89–100.
- Lacour, T., Sciandra, A., Talec, A., Mayzaud, P., and Bernard, O. (2012). Diel variations of carbohydrates and neutral lipids in nitrogen-sufficient and nitrogen-starved cyclostat cultures of *Isochrysis* sp. *J. Phycol.*, 48(4):966–975.
- Narala, R. R., Garg, S., Sharma, K. K., Thomas-Hall, S. R., Deme, M., Li, Y., and Schenk, P. M. (2016). Comparison of microalgae cultivation in photobioreactor, open raceway pond, and a two-stage hybrid system. *Front. Energy Res.*, 4(29).
- Nogales, J., Gudmundsson, S., Knight, E. M., Palsson, B. O., and Thiele, I. (2012). Detailing the optimality of photosynthesis in cyanobacteria through systems biology analysis. *Proc. Natl. Acad. Sci.*, 109(7):2678–2683.
- Nolasco, E., Vassiliadis, V. S., Kähm, W., Adloor, S. D., Ismaili, R. A., Conejeros, R., Espaas, T., Gangadharan, N., Mappas, V., Scott, F., and Zhang, Q. (2021). Optimal control in chemical engineering: Past, present and future. *Comput. Chem. Eng.*, 155:107528.
- Rao, A. V., Benson, D. A., Darby, C., Patterson, M. A., Francolin, C., Sanders, I., and Huntington, G. T. (2010). Algorithm 902. *ACM Trans. Math. Softw.*, 37(2):1–39.
- Underwood, G. J. C., Boulcott, M., Raines, C. A., and Waldron, K. (2004). Environmental effects on exopolymer production by marine benthic diatoms: Dynamics, changes in composition, and pathways of production. *J. Phycol.*, 40(2):293–304.